Aerodynamic and Aerothermal TPS Instrumentation Reference Guide

Bryce A. Woollard[1] and Robert D. Braun[2]
Georgia Institute of Technology, Atlanta, GA 30332

Deepak Bose[3]
NASA Ames Research Center, Moffett Field, CA 95050

The hypersonic regime of planetary entry combines the most severe environments that an entry vehicle will encounter with the greatest amount of uncertainty as to the events unfolding during that time period. This combination generally leads to conservatism in the design of an entry vehicle, specifically that of the thermal protection system (TPS). Each planetary entry provides a valuable aerodynamic and aerothermal testing opportunity; the utilization of this opportunity is paramount in better understanding how a specific entry vehicle responds to the demands of the hypersonic entry environment. Previous efforts have been made to instrument entry vehicles in order to collect data during the entry period and reconstruct the corresponding vehicle response. The purpose of this paper is to cumulatively document past TPS instrumentation designs for applicable planetary missions, as well as to list pertinent results and any explainable shortcomings.

Nomenclature

γ	=	flight path angle
r_n	=	nose radius
r_b	=	base radius
S	=	arc length
R	=	radial length
φ	=	conical half angle
θ	=	circumferential angle
d	=	base diameter
α	=	angle of attack
β	=	sideslip angle
h	=	height
t	=	time
P	=	pressure
T	=	temperature

[1] Graduate Research Assistant, Daniel Guggenheim School of Aerospace Engineering
[2] Professor, Daniel Guggenheim School of Aerospace Engineering, AIAA Fellow
[3] Aerospace Engineering, AIAA Associate Fellow

I. Introduction

Although current hypersonic ground testing facilities are crucial for entry vehicle design, they are limited in their ability to properly model the highly dynamic environments that are associated with the hypersonic entry phase; because of this, many past entry vehicles have incorporated some sort of instrumentation suite to collect *in situ* measurements of the local atmosphere associated with the vehicle during the entry phase. Common measurements taken include surface pressure, surface temperature, TPS recession, and local heat flux – all of which are accomplished through a variety of sensors placed at optimized positions on the vehicle. These measurements allow for 1) a better understanding of the dynamic environment that the vehicle is exposed to during the entry phase, 2) a better understanding of how the vehicle *responds* to that environment, and 3) a reference with which to help validate current models of the dynamic environment such that the margins placed on current vehicle design can be reduced in order to help maximize the overall payload capability of the mission. The compilation of these past configurations allows for a valuable guide to reference when designing any new TPS instrument package. While the remainder of this document will detail each specific mission's instrumentation, Table I through Table IV below summarize the desired measurement parameters and respective instrumentation installed for the planetary missions examined in this survey [32]. It must be noted that while this paper attempts to present a comprehensive document of TPS instrumentation for various planetary missions, it is possible that some details may have been inadvertently missed.

Table I. EDL Instrumentation - Venus Missions.

EDL Instrumentation	Venus	
	Pioneer Venus - Large Probe	Pioneer Venus - Small Probe
TPS/Surface Pressure		
TPS/Surface Temperature	X	X
TPS/Surface Recession		
Heat Flux / Heat Load		
Load / Strain		
Calorimeter		
Shock Layer Radiometer		

Table II. EDL Instrumentation - Earth Missions.

EDL Instrumentation	Earth						
	FIRE II	REENTRY-F	PAET	OREX	MIRKA	ARD	IRVE-3
TPS/Surface Pressure	X	X	X		X	X	X
TPS/Surface Temperature	X	X	X	X	X	X	X
TPS/Surface Recession							
Heat Flux / Heat Load	X	X	X		X		X
Load / Strain							
Calorimeter	X					X	
Shock Layer Radiometer	X		X				

Table III. EDL Instrumentation - HEO Missions.

EDL Instrumentation	HEO				
	Apollo AS-201	Apollo AS-202	Apollo 4	Apollo 6	EFT-1
TPS/Surface Pressure	X	X	X	X	X
TPS/Surface Temperature					X
TPS/Surface Recession					
Heat Flux / Heat Load	X	X			
Load / Strain					
Calorimeter	X	X	X	X	
Shock Layer Radiometer			X	X	X

Table IV. EDL Instrumentation - Mars & Jupiter Missions.

EDL Instrumentation	Mars			Jupiter
	Viking	MPF	MSL	Galileo
TPS/Surface Pressure	X		X	
TPS/Surface Temperature	X	X	X	X
TPS/Surface Recession			X	X
Heat Flux / Heat Load				
Load / Strain				
Calorimeter				X
Shock Layer Radiometer				

II. Data Reconstruction Techniques

While the compilation of raw data from the various instrument packages installed for these missions provides a complete dataset for a particular measureable parameter of entry, descent, and landing (EDL), the ability to truncate, condition, and tailor this data properly is crucial in creating a useful environment reconstruction. Many techniques have been used in the past to accomplish this, such as Kalman Filtering and Multi-Fractional Order Estimation, as well as the Inverse Estimation Methodology proposed by M. Mahzari in [31] for use on the reconstruction of the Mars Science Laboratory (MSL) aerothermal environment. To expand upon the Inverse Estimation Methodology, the fundamental difference between a Direct vs. Inverse Analysis lies within the available parameters with which to examine the problem at hand. For example, in TPS response modeling, if boundary conditions and model parameters are known for a specific application with the goal of obtaining a system's response, a Direct Analysis can be used to estimate the TPS thermal response by measuring its reaction to a defined environment. Conversely, if the response of the system is known relative to an unknown environment, an Inverse Analysis can be used to predict the model parameters and boundary conditions that caused the measured changes in the state of the system[31]. It should be noted that in order to perform a reliable reconstruction using TPS instrumentation, additional information such as inertial rates, vehicle mass properties, and atmospheric properties must also be available.

The purpose for this preface is that while plentiful data may exist for many past planetary missions, the inability to analyze it resultingly limits the usefulness of the data to reduce conservatism in TPS design. Arguably, the development of analysis and reconstruction techniques are almost as critical as instrumenting a vehicle. While beyond the scope of this paper, it is a worthwhile endeavor to evaluate past flight data using state-of-the-art reconstruction techniques.

III. Venus

A. Pioneer Venus (1978)

The Pioneer Venus Mission launched in 1978 was designed specifically to explore the atmosphere of the planet Venus. The mission consisted of three small probes and one large probe which were jettisoned from a bus vehicle at different locations relative to the Venusian atmosphere. Each probe was fabricated with a carbon-phenolic heat shield which varied in thickness due to differing entry flight path angles ($20° < \gamma < 75°$) for each probe. All four probes were 45° sphere-cones with $\frac{r_n}{r_b}$ = 2. While the large probe had a slightly different TPS instrument configuration, all three small probes were manufactured identically. Each small probe included two thermocouple (TC) plugs located at 1) slightly off the stagnation point ($\frac{S}{R}$ = 0.3) and 2) downstream ($\frac{S}{R}$ = 2.2); the large probe TC plugs were located at 1) the stagnation point and 2) at ($\frac{S}{R}$ = 2.2). Each TC plug was fabricated from a cylindrical piece of heat shield material slotted with a 0.062 cm thick ceramic insulator, which included two holes for the TC wires. At the point where the wires protruded from the insulator, the wires were bent such that a 0.002 cm thick junction was flat at the center of the plug. A schematic for the TC plug locations and design is displayed in Figure 1. All plugs were manufactured with Type-K thermocouples (chromel-alumel) and had a maximum service temperature of approximately 1530 K. The large probe TCs were sampled at 2 Hz while the small probes were sampled at 1 Hz. Resistance thermometers were utilized to monitor the cold junction temperatures for each TC plug. All TC plugs were installed in a flat-bottomed hole from the backside of the heat shield, which resulted in all forward plugs to be 0.41 cm below the TPS surface and all aft plugs to be 0.30 cm below the TPS surface[1].

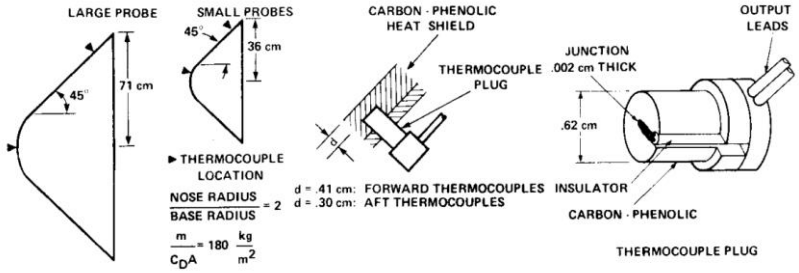

Figure 1. Pioneer Venus Thermocouple Plug Location and Configuration (Ref. XX).

All thermocouple data collected during the probe entries was recovered and reconstructed successfully. While the data from the large probe, day probe, and night probe matched that which was expected, the data from the north probe forward thermocouple indicated a lower rate of temperature rise; this implied that the TPS near the forward thermocouple plug experienced less ablation than expected[1]. More information pertaining to the specifics of the Pioneer Venus Heat Shield Experiment can be found in [1] and [2].

IV. Earth

A. Project Fire-II (1965)

Project Fire was a NASA mission whose aim was to gather in-flight heating data pertaining to the environments associated with Earth entry velocities slightly greater than those of a lunar return. While the overall Project Fire mission included two ballistic test flights, the Fire-I capsule experienced a series of complications during re-entry that drastically altered the gathered dataset and was extremely difficult to dissect. However, the Fire-II mission was very successful, and provided a wide range of data that fed into the design and success of the Apollo missions. The Fire-II forebody was designed as a truncated sphere with a series of three heavily instrumented beryllium layers that could be

ejected on command to expose the next set of thermocouple calorimeters to the freestream flow. Additionally, the second and third beryllium layers were coated with phenolic-asbestos heat shields. The afterbody was manufactured from a fiberglass truncated cone with a phenolic-asbestos and silicon elastomer heat shield that attached to the forebody by means of a bayonet lock. While the Fire-II capsule included a vast range of instrumentation, pertinent sensors for the monitoring of TPS pressure and temperature environments were obtained from 4 radiometers, 144 forebody thermocouples, 12 afterbody gold slug surface thermocouples, and one afterbody static pressure port[3]. Schematics of the forebody instrumentation locations are displayed in Figure 2 and Figure 3, while the afterbody instrumentation locations are displayed in Figure 4. Exact locations of all sensors are documented in both [3] and [4].

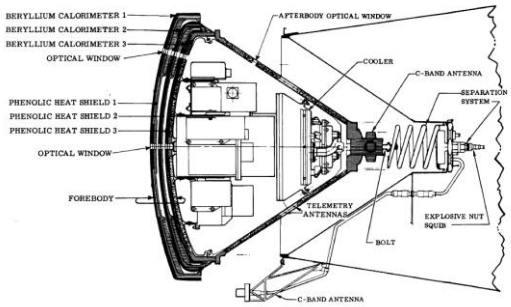

Figure 2. Project Fire-II Vehicle Configuration (Ref. XX).

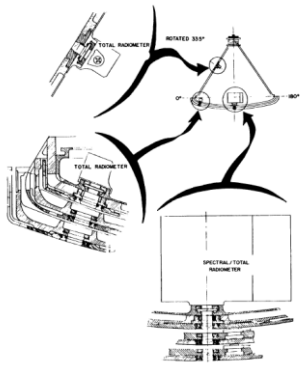

Figure 3. Project Fire-II Radiometer Locations.

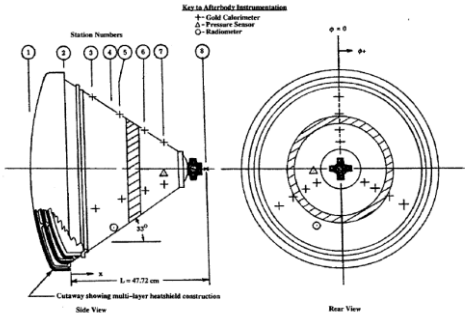

Figure 4. Project Fire-II Afterbody Instrumentation (Ref. XX).

As displayed in the above figures, the Fire-II capsule was instrumented with two different types of radiometers. The lone spectral radiometer and two of the three total radiometers were installed within the beryllium forebody while the remaining total radiometer was installed on the conical afterbody. The spectral radiometer, located at the stagnation point, was designed to operate for a range of heating values of (0.1 – 100 W/cm^2-sr-μ), a range of wavelengths (0.2 – 0.6 μ), and a scan time of 0.1 seconds. All total radiometers were designed as thermopiles with

gold-black-surfaced receivers that operated for a range of heating values from (0.1 – 100 W/cm^2-sr). All systems included in the Project Fire-II radiometer system functioned extremely well during the flight, and the afterbody radiometer confirmed that afterbody heating was primarily convective. A very thorough explanation of the spectral radiometer and total radiometer design, function, operating conditions, and results is documented in [3].

As previously mentioned, the Fire-II vehicle was instrumented with a large number of thermocouples and calorimeters, schematically displayed in Figure 2 and Figure 4. The instrumentation was designed to incur a minimal amount of disturbance on the freestream flow in order to maximize the validity of the dataset. Each of the three beryllium forebody instrument clusters included 12 thermocouple plugs (four variable depth {0.3 mm, 1.8 mm, 3.3 mm, back face} Type-K chromel-alumel thermocouples) within the beryllium calorimeter, as displayed in Figure 5. Note that all thermocouple depths were measured from the front face of the plug where the heat shield was exposed to the freestream.

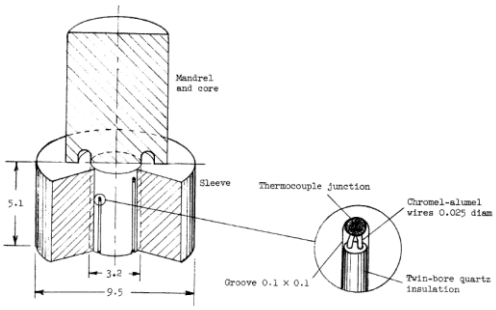

Figure 5. Project Fire-II Beryllium Thermocouple Plugs (Ref. XX).

The plugs were installed within each layer of beryllium in a pattern of four on each of three equally spaced radials. Each plug was press fit from behind into the ablator and the mandrel was machined off to allow the plug to lay flush against the heat shield surface; a detailed manufacturing and installation description for the thermocouple plugs is documented in [3]. Due to the very high number of thermocouples installed in the heat shield, very small lead wires were required (0.075 mm diameter, 0.46 mm sheath diameter); because of this, breakage became a continual problem that limited the number of thermocouples to return any data. The final check-out prior to launch indicated that 21 of the 144 total thermocouples were inoperative due to shorts or breaks. A nearly equal number of thermocouples failed during the actual flight. Luckily, the redundancy of forebody instrumentation redressed this problem [3]. The Fire-II afterbody was instrumented with 12 calorimeters that were comprised of a gold slug mounted within aluminum silicate insulation. This combination acted as the heat sink while Type-K thermocouple junctions (two for redundancy) were attached to the backside of each gold slug to monitor the temperature response [3].

To conclude the Fire-II discussion, the performance of the re-entry system was excellent. Besides the previously mentioned issues concerning disruption of the thermocouple hardware, no further malfunctions were discovered. A complete description of the Fire-II aerothermal instrumentation is documented in [3].

B. Re-entry F (1968)

Launched in 1968, the purpose of Re-entry F was to extend existing turbulent heat transfer data to a high Reynolds and Mach number application, as well as to provide boundary layer transition data for the tested conical geometry. The test vehicle was a 3.962 m (13 ft) slender cone with (φ = 5°) and an initial nose radius of (r_n = 0.254 cm). Thermal measurements were recorded from 21 locations in the beryllium wall, 12 of which were oriented along the primary ray of the vehicle (θ = 0°). Five stations recorded along the diametrically opposite ray (θ = 180°). Additionally, thermal sensors were located at both (θ = 90°/270°) at stations 185.4 cm and 365.7 cm measured from the nose of the cone[5]. Schematics of the Re-entry F temperature, pressure, and heat flux sensors are displayed in Figure 6 and Figure 7.

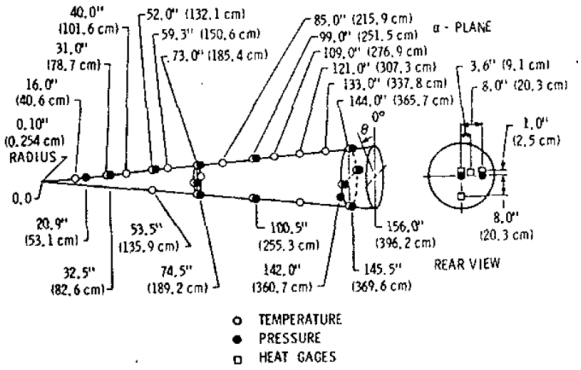

Figure 6. Re-entry F Sensor Locations (Ref. XX).

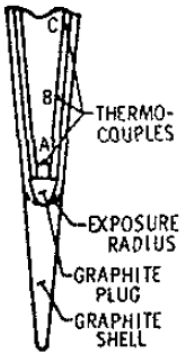

Figure 7. Re-entry F Nose (Ref XX).

At each temperature measurement location, four chromel-alumel thermocouples were spaced at various depths in the beryllium skin, where the outermost thermocouple was embedded 0.0254 cm from the surface. In addition to the TC measurements, 13 pressure orifices were included to help reconstruct the dynamic pressure flow conditions on the vehicle, as displayed in Figure 6. The two pressure sensors and four heat flux gages located on the aft side of the cone were included to help reconstruct the trailing thermal environment. While nearly all of data was successfully returned, the thermocouple at location {x = 185.4 cm, (θ = 270°)} was inoperative at launch and did not return any useful data. A more detailed documentation of the Re-entry F mission can be found in [5].

C. Planetary Atmosphere Experiments Test (PAET) (1971)

The NASA Ames Planetary Atmosphere Experiments Test (PAET) was launched in 1971 to conduct an Earth entry flight that took measurements which aimed to accurately reconstruct the structure and composition of any generic planetary atmosphere. A variety of instruments were utilized during this particular re-entry test, many of which had not previously been tested in flight. The vehicle itself was comprised of a composite forebody sphere-cone and a hemispherical afterbody. The forebody was made up of a blunted beryllium nose with a half angle (φ = 35°), as well as conical frustum with (φ = 55°). The hemispherical afterbody had a base diameter of (d = 0.915 m) and was designed such that all destabilizing moments on the afterbody acted through the vehicle CG[6]. The PAET vehicle configuration is displayed in Figure 8.

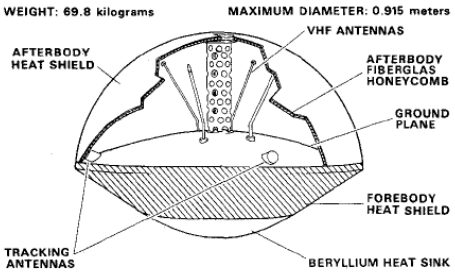

Figure 8. PAET Vehicle Configuration (Ref. XX).

The PAET instrumentation package was comprised of six sensors: two beryllium heat transfer gages (A & B), two forebody heat shield thermocouple plugs (C & D), an afterbody heat shield thermocouple (E), and a forebody pressure gage (F); the locations and sampling parameters of these sensors are displayed in Figure 9.

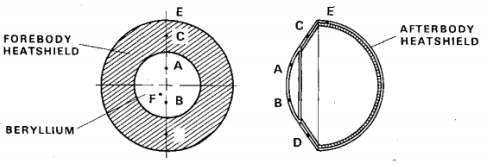

POSITION	COMPONENT	DISTANCE FROM SURFACE n.(cm)	DATA FRAME	RESOLUTION °C	%FS
A	BE	0.025	S	5.1	2.5
B	BE	0.025	S	7.6	2.8
C	F.H.S.	0.330	S,E	9.9	3.3
	F.H.S.	0.635	S	3.2	
	AL	1.02	E	1.9	3.1
D	F.H.S	0.241	S	9.9	1.3
E	A.H.S.	0.660	E	1.9	2.1
F	BE	0	S,E		

S STORAGE: 1 RDG/0.2 sec
E ENGINEERING: 1 RDG/3.2 sec

Figure 9. PAET Sensor Locations and Sampling Parameters (Ref. XX).

The heat transfer gages located at positions A and B were constructed from heritage equipment which was used on both Project Fire-II and Re-entry F. As described in [6], a low-thermal mass thermocouple was desired to be in direct contact with the beryllium, as close to the surface as possible, with a minimum lead wire conduction loss such that the instrument could properly measure the rapid temperature response of the beryllium heat sink. In order to manufacture this, a pre-cooled (-184° C) circular mandrel was inserted in a pre-heated tube (+255° C) where a slot on the mandrel contained a thermocouple bead with 0.0025 cm diameter leads encased in a twin-bore quartz tube. When the assembly was then brought to room temperature, a natural shrink fit occurred between the mating beryllium parts, assuring contact of the thermocouple beads. A section of the top of the assembly was then machined off to produce a flat surface. The entire assembly was then x-rayed to accurately record the location of the sensor relative to the plug. The plugs were then press-fit into their corresponding holes which were machined into the vehicle. A more detailed manufacturing process for the beryllium heat transfer plugs is documented in both [6] and [7]. Additionally, a schematic for the two beryllium heat transfer gages is located in Figure 10.

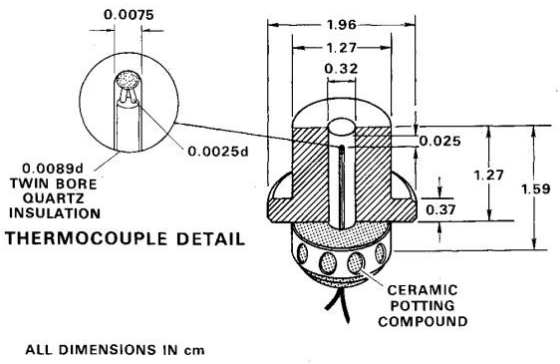

Figure 10. PAET Heat Transfer Gage (Ref. XX).

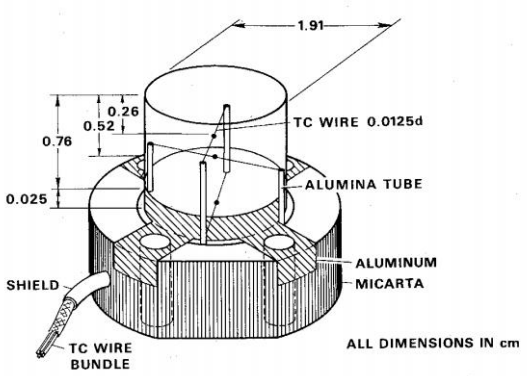

Figure 11. PAET Thermocouple Plug (Ref XX).

The two forebody thermocouple plugs (positions C & D) were an assembly of three components; a cylindrical section of ablative material was bonded to a cylindrical section of aluminum. At the bottom of the assembly was a micarta base in which the TC leads were spliced and redirected toward the vehicle signal conditioner. Two in-depth TCs were positioned in the ablative cylinder at depths equivalent to $\frac{1}{3}$ and $\frac{2}{3}$ of the heat shield thickness. The plugs were fit into machined holes and attached to the PAET vehicle by four screws. Following assembly, the top surfaces of the plugs were sanded down to eliminate any rough edges or discontinuities. A complete detailed description of the manufacturing process for these two TC plugs is documented in [7]; however, a schematic for these plugs is displayed in Figure 11 with corresponding dimensions.

The aftbody thermocouple (E) was butt-welded to the structural honeycomb with a piece of fiberglass. The bonding agent and curing process were identical to that which was used during the fabrication of the structure; therefore, the thermal mass of the system was minimized and the boundary heating conditions were unaltered from

the surrounding structure. Lastly, the dynamic pressure of the forebody was recorded by a lone vibrating diaphragm transducer (F). The particular sensor used in the PAET flight was chiefly attractive due to its absence of zero drift, high temporal resolution, and accuracy over a wide range of pressures (0.001 – 1 atm)[6].

D. Orbital Re-entry Experiment (OREX) (1994)

Launched by JAXA in 1996, the Orbital Re-entry Experiment (OREX) was intended to be a testing platform to provide re-entry data for HOPE, JAXA's equivalent to the Space Shuttle. OREX was launched in 1994, inserted into a singular orbit of Earth, and then commanded to re-enter, collect atmospheric data, and splash down in the central Pacific Ocean. The vehicle itself was a spherically blunted cone with (φ = 50°, r_n = 1.35 m, d = 3.4 m). The TPS used on OREX was a series of carbon-carbon (C/C) tiles, oriented in a circular pattern around a C/C nose, as displayed in Figure 12. The OREX TPS tiles were fitted with a series of thermocouples and platinum resistance thermometers, also displayed in Figure 12. Multiple temperature histories were reconstructed form the TCs in the C/C nose, as well as from locations in the IV quadrant in the radial direction and at the three locations surrounding the C/C nose; a more detailed analysis of the OREX thermal reconstruction is documented in [8] and [9].

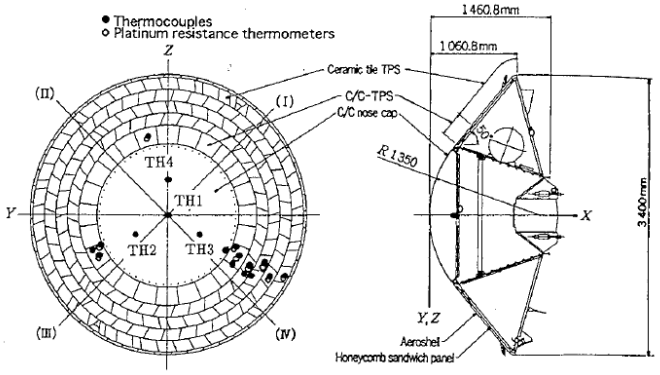

Figure 12. OREX Thermal Sensor Locations (Ref. XX).

E. MIRKA (1997)

The German sponsored MIRKA capsule launched in 1997 was an experimental test flight for a newly developed TPS, called "Surface Protected Ablator", or SPA. The primary scientific goals of the MIRKA capsule were to investigate the re-entry aerothermal environment, verify predicted in-flight temperature histories, and to examine the response of SPA to the imposed re-entry flight conditions. The MIRKA capsule included three main experiments:

- RAFLEX (Rarefied Flow Experiment) – determination of vehicle attitude and aerothermodynamic environment
- PYREX (Pyrometer Re-entry Experiment) – thermal measurement of SPA ceramic outer mold line.
- HEATIN (Heat Shield Instrumentation) – monitoring of the overall TPS response to flight conditions.

While further details of SPA properties are documented in [10], the flight instrumentation aboard MIRKA included two PYREX pyrometers, three RAFLEX pressure probes, and 25 thermocouples (HEATIN), schematically displayed in Figure 13.

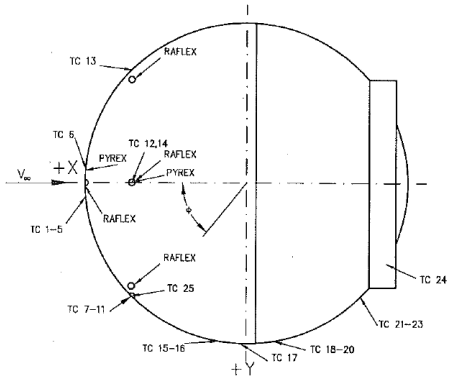

Figure 13. MIRKA Flight Instrumentation Locations (Ref. XX).

As previously mentioned, the MIRKA HEATIN experiment included 25 thermocouples embedded at various depths in the SPA heat shield. Per [10], all TCs were functional during re-entry and returned valuable data with which to perform thermal analysis; however, per [4], it was documented that TCs 15-17 experienced irregular readings likely caused by hot pyrolysis gases upstream. Additionally, the vehicle experienced some unsteady tumbling during re-entry; the lack of an onboard IMU limited the ability to reconstruct the transient angle of attack, so the validity of afterbody data is questionable[4].

F. Atmospheric Re-entry Demonstrator (ARD) (1998)

Launched on October 12, 1998, The Atmospheric Re-entry Demonstrator (ARD) was an ESA sponsored mission that provided the first dataset for a tiled ablative TPS, called Aléastasil (ablative silica fibers impregnated with phenolic resin). The vehicle was a 70% scaled Apollo-like forebody truncated sphere with a slightly modified conical afterbody. The vehicle was instrumented with a series of 28 pressure transducers (15 forebody / 13 afterbody), 15 thermodrums consisting or either three or five thermocouples each, six afterbody surface mounted copper calorimeters, as well as internal structure and RCS nozzle thermocouples[11]. A schematic of the sensor locations on ARD is displayed in Figure 14.

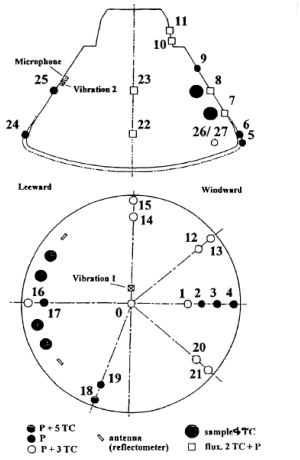

Figure 14. ARD Pressure and Temperature Instrumentation Locations (Ref. XX).

Unfortunately, no useful data was obtained from the afterbody pressure sensors due to a lack of resolution in the instrumentation. Additionally, while the afterbody thermocouples functioned properly throughout the entry, the forebody thermocouples failed above approximately 800°C. Because of this, a heat transfer analysis of the forebody TPS was considered to be impossible; however, the afterbody surface mounted copper calorimeters functioned throughout the entry and provided afterbody heat flux flight data.

Reference [11] provides a more advanced documentation on the ARD vehicle and its design.

G. Inflatable Re-entry Vehicle Experiment 3 (IRVE-3) (2012)

IRVE-3, launched in July 2012, represented NASA's second successful flight test of a Hypersonic Inflatable Aerodynamic Decelerator (HIAD). Following the success of IRVE-II in 2009, the updated science objectives of IRVE-3 were to 1) verify the flexible TPS design through flight demonstration at heat flux environments of at least 12 W/cm^2, and 2) to demonstrate the lifting capability of HIAD in hopes of including a guided entry capability to the flight agenda. As displayed in Figure 15, the IRVE-3 vehicle was manufactured as a series of bound tori that were inflated exo-atmospherically to form a truncated cone that acted as the vehicle's aeroshell during re-entry[12].

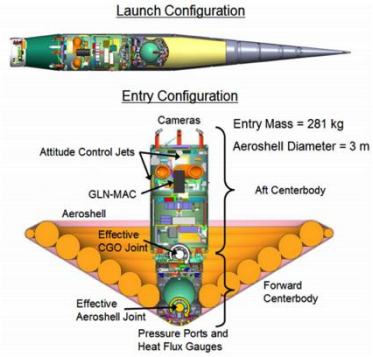

Figure 15. IRVE-3 Vehicle Configuration (Ref. XXX).

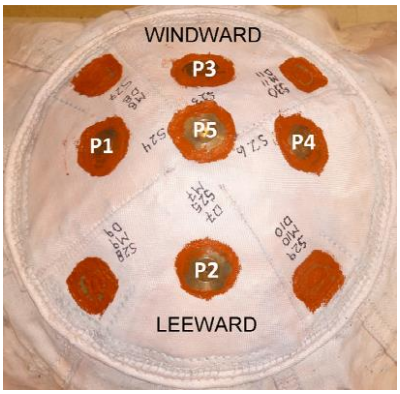

Figure 16. IRVE-3 Pressure Port Locations (Ref. XX).

To permit for reconstruction of both the aerodynamic and aerothermal flight history, the flexible TPS was instrumented with a series of embedded Type-K thermocouples, 5 nose-cap pressure transducers, and 5 nose-cap heat flux sensors. Pressure measurements were obtained from a series of 5 GE® UNIK 5000 pressure transducers located on the rigid blunted nose, as displayed in Figure 16. Each transducer was manufactured from stainless steel, obtained pressure measurements over a range of (1 psi < P < 10,000 psi), and operated over a temperature range of (-55°C < T < 125°C). A complete specification sheet for this series of transducers is documented in [13].

Also collected from 5 locations on the rigid nose, heat flux measurements were obtained from 5 identical MEDTHERM® 64 Series heat flux transducers, displayed in both Figure 17 and Figure 18. Per [14], each transducer provided a self-generated 10 mV (nominal) output at the design heat flux level while continuous readings from 0 to 150% of the design heat flux were collected. The sensors utilized a thermopile to act as the heat sink to which the surface transferred the incoming convective heat flux. A complete data sheet on the MEDTHERM® 64 Series heat flux sensors is documented in [14].

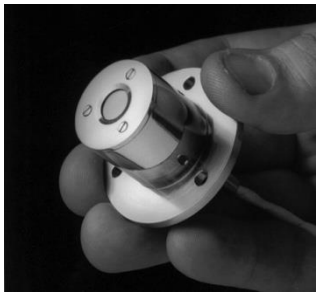

Figure 17. MEDTHERM 64 Series Heat Flux Sensor (1).

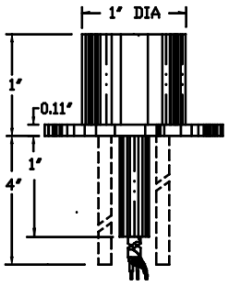

Figure 18. MEDTHERM 64 Series Heat Flux Sensor (2).

V. Human Exploration & Operations

A. Apollo AS-201 & Apollo AS-202 (1966)

The first two suborbital flight tests for the Apollo command module (CM), AS-201 and AS-202, represented NASA's continued efforts toward the planned exploration of the Moon. The specific purposes of the AS-201 and AS-202 missions were to examine the heat rate and heat load responses of the AVCO 5026-39 HC heat shield at orbital re-entry velocities, respectively. Both vehicles were instrumented with a series of pressure transducers and surface-mounted calorimeters at various locations on the heat shield, the forward compartment, and the crew compartment, as displayed in Figure 19 and Figure 20. Each heat shield was instrumented with 12 pressure transducers and 12 calorimeters while each conical afterbody was instrumented with 24 pressure transducers and 23 calorimeters; the exact coordinates of each sensor are listed in Table V and Table VI[15]. Note that filled-in symbols in Figure 19 and Figure 20 represent sensors that were either inoperative or provided unreliable data during flight testing.

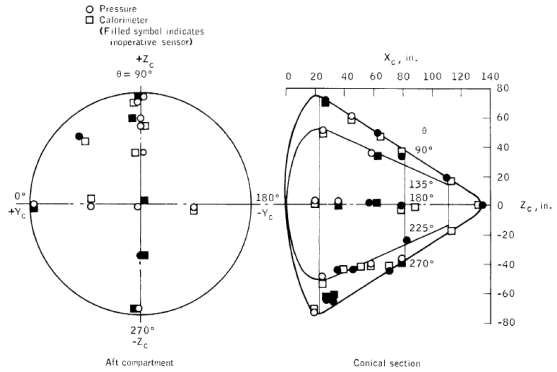

Figure 19. AS-201 Pressure Transducer and Calorimeter Locations (Ref. XX).

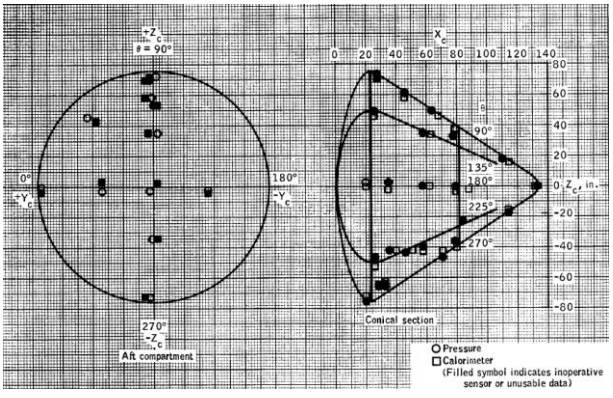

Figure 20. AS-202 Pressure Transducer and Calorimeter Locations (Ref. XX).

Table V. AS-201 & AS-202 Pressure Transducer and Calorimeter Locations (Heat shield) (Ref. XX)

Pressure Sensor			Calorimeter		
Y_c (in)	Z_c (in)	Range (psia)	Y_c (in)	Z_c (in)	Range (Btu/ft^2-s)

		AS-201	AS-202			
0.0	75.0	0 - 10	0 - 5	1.3	74.7	300
2.3	-71.8	0 - 10	0 - 3	4.8	-71.8	200
2.3	70.5	0 - 17.5	0 - 5	4.0	71.8	300
71.8	-0.8	0 - 15	0 - 3	71.8	-3.3	200
0.0	58.4	0 - 17.5	0 - 5	4.8	58.4	300
0.0	54.4	0 - 17.5	0 - 5	-2.0	56.3	200
-2.1	35.2	0 - 17.5	0 - 5	4.0	33.3	250
0.0	-35.0	0 - 10	0 - 3	-2.7	-35.0	200
34.3	-2.1	0 - 10	0 - 5	39.0	4.6	200
-36.7	-3.8	0 - 10	0 - 5	-38.6	-5.7	200
6.0	-2.5	0 - 10	0 - 5	-0.2	0.6	250
42.4	45.9	0 - 10	0 - 5	41.1	44.4	300

Table VI. AS-201 & AS-202 Pressure Transducer and Calorimeter Locations (Conical Afterbody) (Ref. XX)

Pressure Sensor			Calorimeter		
X_c (in)	θ (deg)	Range (psia)	X_c (in)	θ (deg)	Range (Btu/ft^2-s)
26.5	91.8	0 - 3	26.5	93.7	100
45.5	88.1	0 - 3	45.5	85.3	50
62.3	93.4	0 - 3	64.8	92.0	50
78.9	118.2	0 - 3	78.9	115.0	50
110.0	95.8	0 - 3	114.0	83.4	50
25.3	136.1	0 - 3	25.3	138.0	50
19.4	271.6	0 - 3	19.4	270.0	10
82.6	219.8	0 - 3	88.0	182.9	25
19.4	177.0	0 - 3	19.4	178.5	25
25.3	223.5	0 - 3	25.3	225.5	10
78.9	187.9	0 - 3	78.9	191.3	25
37.5	215.3	0 - 3	40.0	215.3	10
78.9	263.9	0 - 3	78.9	267.8	25
114.0	275.0	0 - 3	114.0	265.0	25
45.5	226.0	0 - 3	51.7	229.8	10
59.0	142.8	0 - 3	61.5	142.8	25
35.0	176.5	0 - 3	35.0	178.6	25
57.4	177.6	0 - 3	60.0	177.5	25
70.5	271.9	0 - 3	70.5	276.4	25
133.0	Apex	0 - 3	133.0	Apex	25
58.0	232.0	0 - 3	58.0	234.0	25
27.1	253.0	0 - 7	27.1	253.0	25
32.6	253.0	0 - 7	32.6	253.0	50
32.6	253.0	0 - 7			

Two different types of calorimeters were used to measure surface heating on the vehicle; asymptotic calorimeters, schematically displayed in Figure 21, were installed on the conical afterbody of the CM to measure heating rates less than 50 Btu/ft^2-s. Conversely, high-range slug calorimeters (Figure 22) designed specifically for the Apollo program were installed on the heat shield to measure heating rates greater than 50 Btu/ft^2-s. The high-range slug calorimeters were constructed from several graphite wafers that were stacked to allow for *in situ* heating measurements to be taken during the surrounding heat shield ablation[15]. A more detailed description of the design and operation of the two types of calorimeters can be found in [16] and [17], respectively.

Six of the twelve high-range calorimeters on the AS-201 heat shield were operational, and data was recorded from entry to 54 seconds after entry; however, post-processing exposed that heat losses to subsequent wafers and surrounding material was so prominent that none of the heating results were considered useful[15]. The AS-201 conical afterbody asymptotic calorimeters (Figure 19) returned data from 16 of the 23 locations; however, the heating data showed a series of irregularities between 1580 seconds and 1635 seconds, which are assumed to be attributed to the recording circuitry. Following peak heating (1635 seconds), the main electrical bus began to show transient drifting from expected heating values until the entire electrical system shorted out at 1650 seconds, causing a loss of data[15]. A deeper analysis of the conical afterbody heating results from the AS-201 test flight is located in both [4] and [15].

Unfortunately, the AS-202 heat shield calorimeters also experienced numerous malfunctions, such as thermocouple shorting and premature switching from each wafer, so no useful heat shield heating data was collected from the test flight. As for the conical afterbody heating data from AS-202, besides a temporary loss of data due to heat rates exceeding the sensor design limits, useful data was returned from 19 of the 23 calorimeters and an aerothermal reconstruction of the re-entry environment was conducted. A specific analysis of the AS-202 afterbody heating is located in [18].

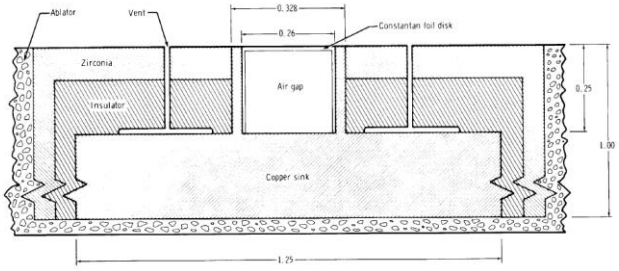

Figure 21. AS-201 & AS-202 Asymptotic Calorimeter Schematic (Ref. XX).

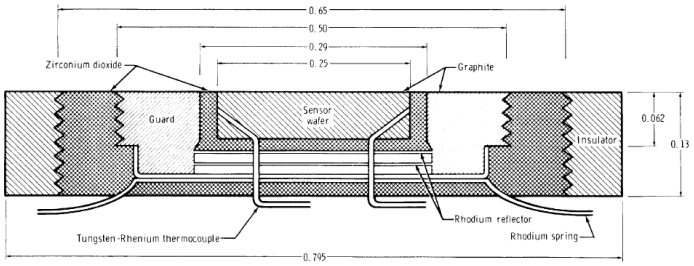

Figure 22. AS-201 & AS-202 High-Range Slug Calorimeter Schematic (Ref. XX).

As previously mentioned, pressure measurements were taken from a collection of 36 pressure transducers located at various locations on the Apollo test vehicles. For AS-201, useful flight data was obtained from 19 operative pressure sensors (10 on the heat shield, 9 on the afterbody). While the recorded flight data from the heat shield matched up very well with the estimates made from previously conducted wind-tunnel experiments, the data obtained from the conical pressure transducers did not. This lack of resolution was attributed to the choice of afterbody pressure sensors. As displayed in Table VI, most of the conical pressure transducers installed had a pressure domain of 0 – 3 psia; however, the maximum pressure that the conical sensors were anticipated to be exposed to was only 0.5 – 1.0 psia[15]. Additionally, the scimitar antenna disturbed the flow near many pressure sensors, generating a fictitious

dataset. As for AS-202, flight data was obtained from 10 of 12 pressure transducers on the heat shield and only one transducer located on the toroid. For unknown reasons, no measureable pressure rise was detected on the conical afterbody until just before parachute deployment; therefore, none of the afterbody pressure data was considered useful.

All flight measurements were recorded on a magnetic tape aboard each spacecraft. While the entire dataset for AS-202 was successfully recovered, an electrical power subsystem malfunction on AS-201 caused a permanent loss of heating-rate data approximately 86 seconds after entry[15].

B. Apollo 4 (1967) & Apollo 6 (1968)

While the purposes of AS-201 and AS-202 were to respectively examine the heat rate and heat load responses of the AVCO 5026-39 HC heat shield, the purposes of both Apollo 4 and Apollo 6 were simply to qualify the entire flight system for lunar return velocities. Due to these superorbital entry velocities, radiative heating became a subject of concern and new instrumentation needed to be included on the vehicles. Heritage flight instrumentation, specifically the wafer calorimeter design used on the heat shields of AS-201 and AS-202, was modified for the Apollo 4 and Apollo 6 missions due to the malfunctions associated with the AS-201 and AS-202 hardware. Both vehicles were instrumented with 17 pressure transducers, four radiometers, and 32 calorimeters, as displayed in Figure 23. The exact locations of these sensors are documented in [19].

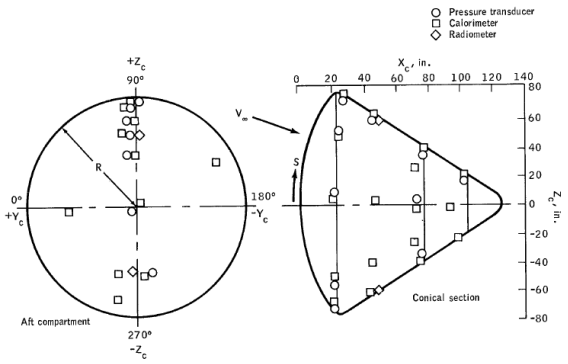

Figure 23. Apollo 4 & Apollo 6 Instrument Locations (Ref. XX).

The installed pressure transducers collected data through pressure ports in the vehicle that led to a standard strain gage diaphragm located within the structure, schematically displayed in Figure 24. While all transducers on the conical afterbody were only designed to record static pressures up to 2 psia, two of the seven pressure sensors on the heat shield were able to gather pressure data up to 5 psia while the other five allowed for pressures up to 10 psia[19]. Both Apollo 4 and Apollo 6 were able to return a successful pressure dataset from the aforementioned instrumentation; a further analysis of the results is documented in [19].

As previously mentioned, four radiometers were installed on the Apollo vehicles due to the expectation for radiative heating at superorbital entry velocities. The instrumentation, schematically displayed in Figure 25 and Figure 26, was configured as an embedded thermopile located within the ablator material behind a quartz window. The maximum diameter of each radiometer was approximately 1 inch and the viewing angle was altered in conjunction with the radiometer location (7° on the heat shield, 30° on the conical afterbody). While both vehicles had radiometers installed on the conical afterbody, no radiative heating response was recorded from either vehicle; this was not a hardware malfunction, but in fact confirmed the predictions that the conical afterbody would not experience any radiative heating. For Apollo 4, the heat shield radiometer located off-stagnation was inoperative at the time of launch and did not record any flight data; however, the radiometer at the stagnation point functioned properly for a majority of the time domain (discrepancies at peak heating and after t = 30,050s) and returned a dataset which was in good agreement with the radiative heating predictions. As for Apollo 6, errors in the entry flight velocity caused the radiative heating results to be an order of magnitude lower than what was expected. Additionally, the raw data from the heat shield radiometers had a noise level which was nearly as prominent as the actual measurements; a post-flight inspection exposed a small obstruction in the radiometer port which was most likely the cause for the inconsistencies[19].

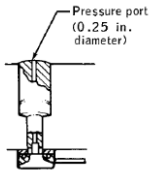

Figure 24. Apollo 4 & Apollo 6 Pressure Transducer Schematic (Ref. XX).

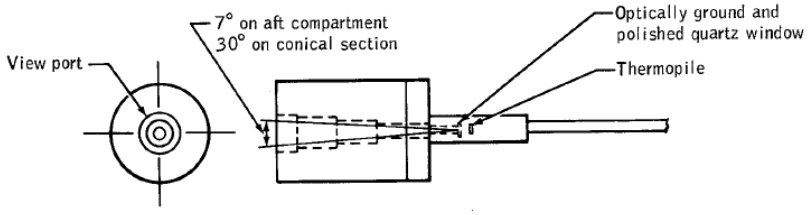

Figure 25. Apollo 4 & Apollo 6 Radiometer Schematic (1) (Ref. XX).

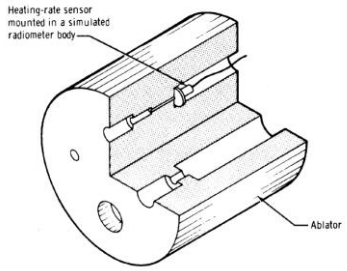

Figure 26. Apollo 4 & Apollo 6 Radiometer Schematic (2) (Ref. XX).

Similar to AS-201 and AS-202, two types of calorimeters were installed on the Apollo test vehicles. Eleven wafer calorimeters were utilized on the heat shield while 21 asymptotic calorimeters were installed on the conical afterbody; however, the numerous malfunctions that occurred during the previous two test flights prompted the re-design of the heat shield wafer calorimeters, schematically displayed in Figure 27. The re-design proved to be successful, as both test vehicles were able to return a heating dataset which matched relatively well with convective heating estimates. Additionally, the afterbody asymptotic calorimeters (Figure 28) functioned relatively well and provided a dataset with values near the cold wall predictions; a more thorough explanation of the afterbody results is documented in both [4] and [19].

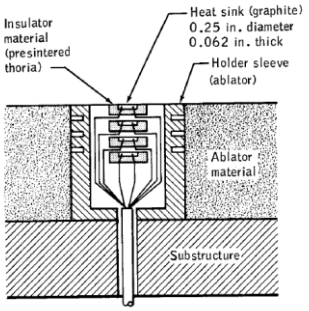

Figure 27. Apollo 4 & Apollo 6 Heat Shield Wafer Calorimeter Schematic (Ref. XX).

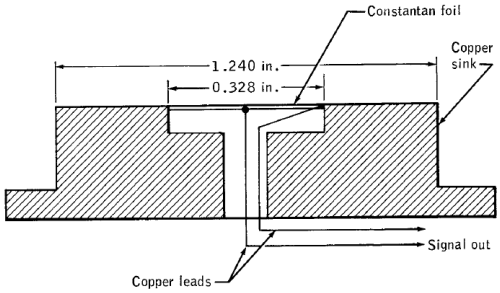

Figure 28. Apollo 4 & Apollo 6 Asymptotic Calorimeter Schematic (Ref. XX).

C. Orion Exploration Flight Test-1 (EFT-1) (2014)

Orion Exploration Flight Test-1 (EFT-1) was the first re-entry flight test of NASA's next generation human spaceflight capsule. Similar to Apollo, Orion entry capsule has a spherical section forebody with Avcoat, an epoxy novolac resin system embedded in a fiberglass honeycomb matrix as the TPS. The vehicle is, however, larger than Apollo: 5 m vs. 3.5 m diameter. The afterbody TPS is built from shuttle tiles. EFT-1 flight profile was design for an atmospheric entry speed of 8.9 km/s and -12.6 degree flight path angle. The vehicle flew a guided hypersonic re-entry trajectory at L/D=0.25 to meet landing accuracy requirements. One of the primary objectives of the flight test was to validate model predictions of aerodynamics, aerothermodynamics, and the design of the thermal protection system. The heatshield and the backshell were instrumented with temperature, pressure, shock-layer radiation sensors. On the heatshield TPS, 34 instrumented plugs similar to instrumented plugs flown on Mars Science Laboratory (MSL) (discussed in section VI) were used. The 1.3-in diameter plugs were made from Avcoat, and contained multiple thermocouples at various depths to provide data for aeroheating reconstruction and in-depth thermal performance. Figure 29 shows images of the Avcoat instrumented plugs. The number, type, and depths of the thermocouples in each plug were customized according to local aerothermal environment to extract maximum value from the data. Depending on the primary objective, the plugs were divided into two classes: 19 Thermal Plugs and 15 Aerothermal Plugs. The Thermal Plugs contained 4 TCs each while the Aerothermal Plugs were instrumented with only two near surface thermocouples. The Thermal Plugs also contained a HEAT (Hollow aErothermal Ablation and Temperature) sensor similar to the sensor used in the instrumented plugs on MSL discussed later in Sec. VI C. The instrumented plugs were installed strategically as shown in Fig. 30 (a) to answer questions associated with key aerothermal phenomenon such as stagnation heating, boundary layer transition, turbulent heating augmentation, shoulder heating, and augmentation due to the presence of compression pads. Signatures of some key aerothermal phenomena are observed on the surface of the recovered vehicle as shown in Fig. 30 (b). In addition to thermal and aerothermal plugs, two broadband radiometers were also installed to measure shock layer radiation. The radiometers used a window less port on the TPS with an embedded sapphire rod leading to a thermopile sensing element. As shown in Fig. 30 (a), one radiometer was installed near the stagnation region, and the second radiometer was installed on the leeside forebody region on the pitch plane.

Nine Flush Air Data System (FADS) ports were also installed to measure surface pressure during reentry also shown in Fig. 30 (a). Tubing from each 0.15" FADS port on the heatshield led to a Honeywell PPT pressure transducer. The layout of the FADS port allowed reconstruction of wind relative vehicle attitude, vehicle aerodynamic forces, and atmospheric density.

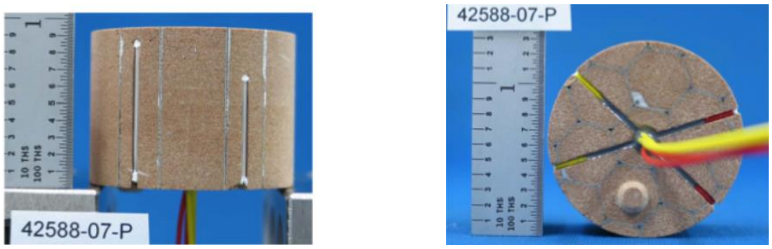

Figure 29. Avcoat Instrumented Plugs for EFT-1 (a) Side View, and (b) Bottom View

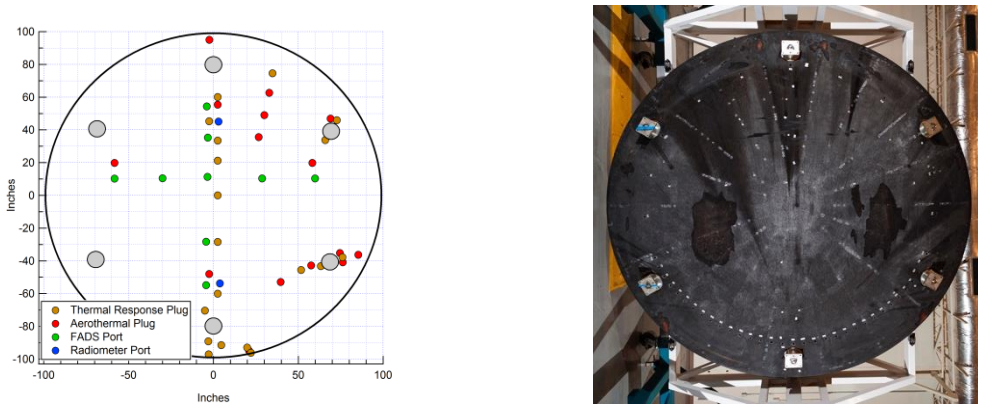

Figure 30. (a) EFT-1 Heatshield Instrumentation Layout, and (b) Recovered EFT-1 Heatshield

EFT-1 backshell TPS tiles included several pressure transducers, surface thermocouples, and in-depth TCs for assessments of backshell heating and pressure environment. Several flight test objectives such as catalytic overshoot, micrometeoroids and orbital debris cavity damage assessment, heating augmentation around various features, and backshell contribution to aerodynamics were supported by using backshell instrumentation.

The instrumentation system performed successfully and useful data were obtained. The analysis of the data is currently being used to update predictive models. A few anomalies in the data have also been identified. The near surface thermocouples show a noisy response during a portion of the flight when they get closer to the surface due to recession. An investigation is currently underway to identify the root cause of the noise, which appears to correlate with vehicle angle of attack changes. A solution to this problem is being developed for the next Orion test flight. Anomalous data were also obtained from the HEAT sensor response. This anomaly is partially explained by an electrical ground loop path through the conductive char layer. A lack of recession data was identified as a shortcoming that reduced the reconstruction accuracy. The radiometer data also exhibited some anomaly due to the radiation generated by the hot internal surfaces of the port through the TPS. An analytical compensation was used to explain the measured data.

VI. Mars

A. Viking 1 & 2 (1976)

The Viking missions launched in 1976 represented the first successful landings by the United States on the surface of Mars. Two geometrically identical vehicles (VL1 & VL2) were launched and entered the Martian atmosphere at different locations. The vehicles were comprised of a 3.5 m diameter blunted cone aeroshell (φ = 70°, $\frac{r_n}{r_b}$ = 0.5) and a bi-conic afterbody, as displayed in Figure 31. The vehicle flew a lifting entry with a lift-to-drag ratio of 0.18 at $\alpha \approx 11.1°$. The inner cone afterbody was fabricated from glass fabric and phenolic resin, while the outer cone afterbody was constructed from aluminum alloy. While the aeroshell was equipped with ablative SLA561-V TPS, the bi-conic afterbody was not manufactured with any ablative TPS due to a small afterbody heat flux estimate[20].

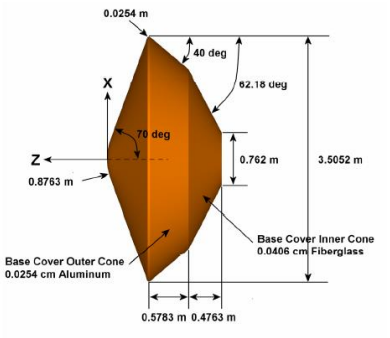

Figure 31. Viking Aeroshell and Backshell Geometry (Ref. XX).

Both VL1 and VL2 were instrumented with both pressure and temperature sensors; included on the forebody aeroshell were four pressure sensors oriented in a circular pattern about the nose (R = 50 in), as well as a stagnation pressure port just downstream of the aeroshell apex (Figure 32). The purpose of the four pressure sensors was to monitor the vehicle's angle of attack (α) and sideslip angle (β) through the entry corridor; however, due to inconsistent data points, the data received from these ports was considered unreliable. Possible causes for this discrepancy, besides instrumentation errors, included high speed thermochemical non-equilibrium at opposing pressure port locations, Newtonian flow effects, and local surface ablation changes. A further description of the pressure data set can be found in [21].

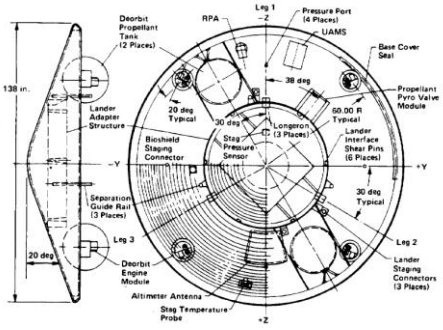

Figure 32. Viking Aeroshell Instrumentation (Ref. X).

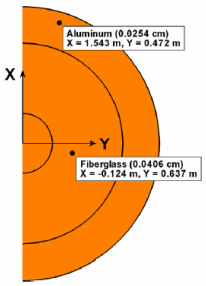

Figure 33. Viking Backshell TC Locations (Ref. X).

While the forebody TPS was not instrumented with any thermocouples, there were a total of five temperature sensors installed on the aeroshell - two on the backface of the aeroshell and one on each of the bases of three components that protruded through the aeroshell surface. These components include the radar antenna, the stagnation pressure port, and the stagnation temperature probe; the location of these five temperature sensors allowed for an inboard, outboard, and intermediate temperature history for the backside of the aeroshell. The exact location of these components is also displayed in Figure 32. The composite Viking backshell was instrumented with two thermocouples, one in each material, as displayed in Figure 33. While both TCs functioned properly on VL2, the outer TC located on the aluminum conic section for VL1 failed before it reached its peak value. A more detailed description of the Viking temperature history is located in [20].

B. Mars Pathfinder (MPF) (1996)

Mars Pathfinder, launched by NASA in 1996, represented a low-cost demonstration for placing a science payload, and more specifically a rover, on the Martian surface. The entry vehicle was a 2.65 m diameter, 70° sphere cone with (r_n = 0.66 m). The aeroshell was manufactured with ablative SLA561-V TPS and was instrumented with nine Type-K thermocouples (TC1 – TC9) and three platinum resistance thermometers (PRT1 – PRT3), as displayed in Figure 34[22].

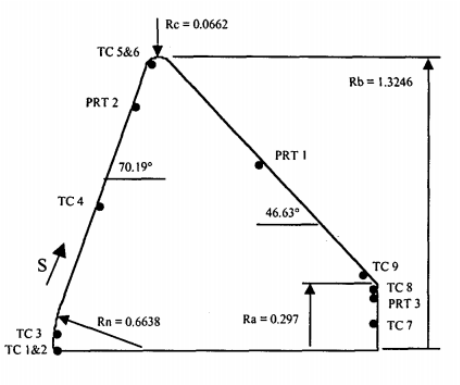

Figure 34. Mars Pathfinder TC and PRT Locations (Ref. XX).

As documented in [22], the thermocouples utilized thin wires that were installed parallel to the aeroshell surface in order to minimize temperature lag and heat conduction on the leads. TC1 – TC3 were installed in the vicinity of the aeroshell apex at various depths, TC4 was installed at the bondline nearly halfway up the conical frustum, TC5 and TC6 were installed at the shoulder at various depths, and TC7 - TC9 were located on the backshell below the surface of the SIRCA tiles. PRT1 was located at the bondline nearly halfway down the backshell, while PRT2 and PRT3 were both attached to aluminum blocks inside the vehicle which served as the reference junction for the nine thermocouples. The exact locations and depths of all thermal sensors are listed in Table VII.

Table VII. Mars Pathfinder Thermal Instrumentation Locations (Ref. XX).

Sensor	R (cm)	S (cm)	Depth (cm)
TC1	0.00	0.00	0.400
TC2	0.00	0.00	0.953
TC3	7.62	7.64	1.905
TC4	66.44	69.7	1.905
TC5	130.4	138.0	0.953
TC6	130.4	138.0	1.905
TC7	12.0	N/A	0.038
TC8	27.6	N/A	0.038
TC9	34.0	N/A	0.038
PRT1	83.9	212.50	1.340
PRT2	110.0	Inside Structure	
PRT3	23.5	Inside Structure	

The thermal instrumentation had a variable sampling rate that ranged from 0.125 Hz at initiation to 1 Hz at 78 seconds after initiation. Per an in-flight vehicle health check, data suggests that TC1, TC7, and TC8 failed before or during launch; however, the remaining thermocouples and PRT1 measured a positive temperature gradient that can be attributed to aerothermal heating. PRT3, which was attached to one of the two aluminum blocks inside the structure, showed no change in temperature as expected. PRT2, which was attached to the other aluminum block, recorded a constant temperature reading of 233.3 K throughout entry; this dataset is incorrect, however, because these measurements were located at the low-temperature cutoff for the calibration curve. Because of this, the raw data from TC2 – TC6 was inaccurate (reference junction discrepancy), but the dataset was able to be corrected using results from solar thermal vacuum (STV) tests prior to launch. A complete analysis of the Mars Pathfinder aerothermal

reconstruction and heat shield material response is documented in [23].

C. Mars Science Laboratory (MSL) (2012)

Launched in 2011, NASA's Mars Science Laboratory (MSL) brought a wide new spectrum of technologies and capabilities to the entry, descent, and landing (EDL) field. In addition to the introduction of Skycrane and the ability of the rover, *Curiosity*, to land on its own wheels, the MSL heat shield was heavily instrumented in order to capitalize on the testing domain provided by the hypersonic and supersonic entry. The Mars Science Laboratory (MSL) Entry Descent and Landing Instrumentation (MEDLI) suite equipped on the MSL aeroshell was able to record pressure, temperature, and in-depth isotherm from the phenolic-impregnated carbon ablative (PICA) heat shield. MEDLI was broken into two distinct experiments, the first being a combination of 1) the MEDLI Integrated Sensor Plug (MISP) and the Hollow aErothermal Ablation and Temperature (HEAT) sensor and 2) the Mars Entry Atmospheric Data System (MEADS). The purpose of MISP was to help better understand the temperature gradients through PICA during the Mars entry phase. In order to accomplish this, each MISP plug configuration included 4 Type-K (chromel-alumel) thermocouples with a 0.012" wire diameter embedded at various depths (0.254 cm, 0.508 cm, 1.143 cm, 1.778 cm) in a small pillbox (d = 1.3 in, h = 1.14 in) of PICA[24]. As MSL descended through the Mars atmosphere, each thermocouple recorded the *in situ* temperatures through the plug, therefore providing a dataset for the thermal material response of PICA at the Mars specific heating conditions. The MISP plug configuration is displayed in Figure 35, while the locations of the seven MISP plugs on the MSL heat shield are displayed in Figure 37.

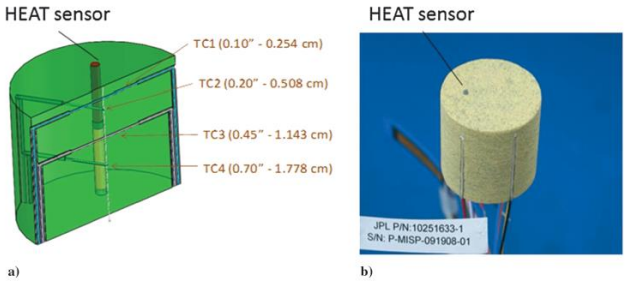

Figure 35. a) MISP Plug Configuration and b) HEAT Sensor Location in MISP Plug (Ref. XX).

The purpose of a HEAT sensor was to track a temperature isotherm as a surrogate for TPS recession through the entry pulse in order to better understand the material response of PICA in Mars specific heating conditions. In order to accomplish this, each HEAT sensor consisted of a series of wound resistive wires embedded in an insulation barrier which utilized the conductive char layer to "complete the circuit", as displayed in Figure 36. The *in situ* resistance associated with the circuit was directly proportional to the length of the wire, which decreased as the char layer ablated toward the aeroshell, and was intended to provide the progression of a temperature isotherm. The HEAT sensor data obtained, however, was anomalous due to a faulty ground loop, and could not be used for analysis. The recession of the TPS was, however, bounded to a value less than 0.1" since all near surface TCs survived the heat pulse.

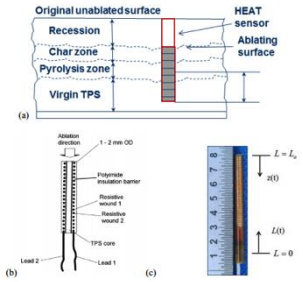

Figure 36. a, b) HEAT Sensor Schematic and c) HEAT Sensor (Ref. XX).

Lastly, MEADS's science objective was to reconstruct hypersonic aerodynamic performance and atmospheric density for MSL entry. MEADS was designed to collect estimates of the freestream Mach number (M_∞), dynamic pressure (q_∞) greater than 850 Pa to within ±2%, and the angle of attack (α) and sideslip angle (β) to within ±0.5°. Additionally, the positioning of the seven MEADS pressure ports allowed for an overall pressure distribution of the aeroshell to be reconstructed. In order to accomplish this, MEADS collected data through 7 pressure transducers located in a cross pattern on the heatshield, as displayed in Figure 37[25]. Additional documentation on the MSL MEDLI flight system can be found in [26] and [27].

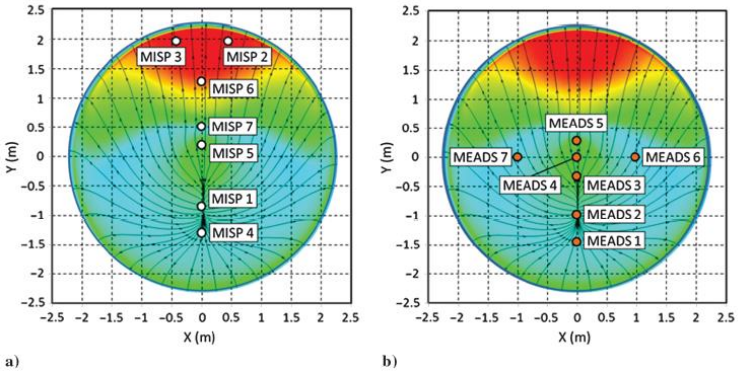

Figure 37. a) MISP and b) MEADS Port Locations (Ref. XX).

VII. Jupiter

A. Galileo (1995)

The launch (1989) and entry (1995) of NASA's Galileo probe represents the first and only successful attempt to enter and examine the Jovian atmosphere. A significant obstacle of this specific mission was the intense heating environment that Galileo was projected to encounter, with as estimated peak heat flux of 17 kW/cm^2. The Galileo entry vehicle was designed and manufactured as a (φ = 45°) sphere cone with a forebody carbon-phenolic heat shield and a phenolic-nylon afterbody. The probe was instrumented with four embedded resistance thermometers and ten Analog Resistance Ablation Detector (ARAD) sensors, schematically displayed in Figure 38 and Figure 39. As displayed in Figure 40, each resistance thermometer was manufactured from an octagonal piece of aluminum and bonded to the interior of the structure by means of Eccobond 57C - a high density, electrically conductive epoxy. Each thermometer contained a small nickel sensing element which was designed to record temperatures ranging from 250 K to 450 K. All resistance thermometers were sampled at 0.125 Hz and only six values were planned to be stored at any given time in a recyclable fashion. While the thermometers were programmed to stop taking measurements at the same time as the ARAD sensors (t = 110 s), the switch to terminate thermal data recording was never engaged due to unintended command sequences and the earlier entry data (including the initial cold-soak temperatures) was overwritten by future data; therefore, the only thermal data set covers the temporal domain of approximately 120s < t < 160s[28]. More information about this software glitch can be found in [29], while a further analysis of the thermal dataset is located in [28].

Each ARAD sensor, displayed in Figure 41, was essentially an earlier iteration of the previously described HEAT sensor (Figure 36) instrumented on the Mars Science Laboratory (MSL). Each ARAD sensor was to be installed within the TPS and ablate parallel to the heat shield while utilizing the conductive char layer to "complete its circuit". Due to the direction of ablation, the decreasing circuit length was then directly proportional to the circuit's resistance, so a current could be fed through the circuit and a resulting resistance and voltage could be recorded. Each ARAD sensor was sampled at an average of 1.75 Hz and data was passed through an analog-to-digital converter to be stored as 8-bit binary numbers in recycling memory. This allowed each ARAD sensor to span the ablative domain of flight and successfully collect 84 data points[30]; a more detailed explanation and review of the Galileo heat shield ablation system is located in [30].

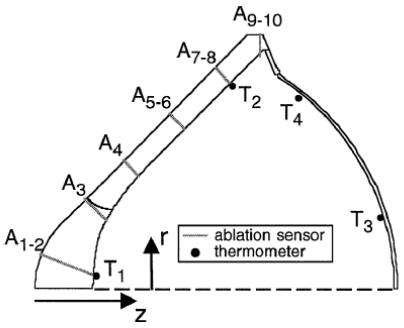

Figure 38. Galileo Flight Instrumentation Locations (Ref. XX).

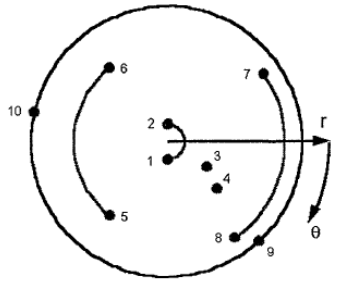

Figure 39. Galileo ARAD Sensor Locations (Ref. XX).

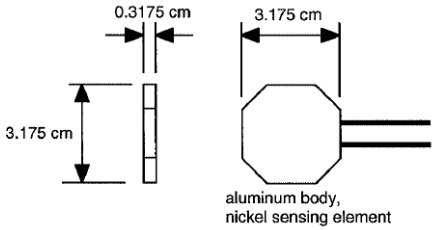

Figure 40. Galileo Resistance Thermometer Schematic (Ref. XX).

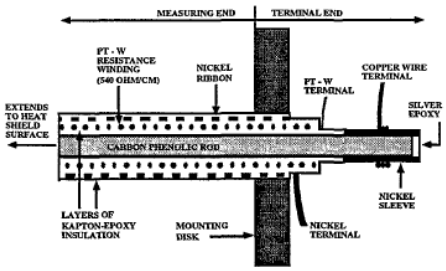

Figure 41. Galileo ARAD Sensor Schematic (Ref. XX).

VIII. Future Instrumentation Considerations

It is clear from the variety of instrumentation packages installed on the wide range of missions surveyed in this document that having an assortment of instrumentation options aids greatly in optimizing the system's capability to obtain desired data while minimizing its footprint on the flight vehicle. Although most of the technologies included in this survey are products of heritage military research stemming from the "Space Race", modern advancements in sensor, data, and communication systems provide unique opportunities for future instrumentation packages. Also, due to multidisciplinary application of sensor systems, significant leverage is possible via adoption of know-how from industries with similar measurements and/or reliability requirements, such as aviation, automobile, energy, medical, and consumer electronics. Future instruments must exploit technology advancements especially in sensor miniaturization, low power and passive sensors, wireless and modular data systems, etc. For example, the continual development and shaping of microelectromechanical systems (MEMS) technology may provide an entirely new

range of instrumentation possibilities, specifically related to minimizing mass and volume parameters that impose hard constraints in some missions.

In addition, cost of sensor implementation must be reduced by developing and pre-qualifying sensor systems for a variety of missions and offering them as a commodity. New and customized solutions, while optimal, are often expensive and introduce risk to the mission which can be difficult to retire in a timely manner. Increased reliance on commercial components, where possible, by trading some robustness requirements also has the potential to significantly reduce cost.

Finally, sensors themselves must be developed and adapted to meet the demands of more extreme entry environments and increased accuracy. Since sensors are integrated in a TPS material, it must also be continually adapted and developed for new ablative systems. Recently developed material systems such as woven and conformal TPS pose integration challenges even for existing flight-proven sensors.

IX. Concluding Remarks

Acquiring entry system performance data using instrumentation is critical for advancement of system capability and risk reduction, as demonstrated by several instrumented flight missions. This paper documents key hardware details of TPS instrumentation of NASA's planetary entry systems, the data acquired, and some anomalies observed. The rich set of flight data has formed the foundation for improvements in modeling, ground testing, and overall TPS design reliability for a variety of planetary missions. The examples of failures and anomalies are also highlighted in order to derive lessons for future improvements. Future opportunities in improvements of flight instrumentation are also discussed especially in regards to areas of technology advancements, cost reduction, and integration with new TPS materials.

X. References

[1] Wakefield, R. M. and Pitts, W. C., "Analysis of the Heat-Shield Experiment on the Pioneer-Venus Entry Probes," 1978.

[2] Ahn, H. K, Park, C., and Sawada, K., "Response of Heatshield Material at Stagnation Point of Pioneer-Venus Probes," *Journal of Thermophysics and Heat Transfer*, Vol. 16, No. 3, 2002.

[3] Richardson, N. R., "Project Fire Instrumentation for Radiative Heating and Related Measurements," NASA TN D-3646, 1966.

[4] Wright, M. J., Milos, F. S., and Tran, P., "Survey of Afterbody Aeroheating Flight Data for Planetary Probe Thermal Protection System Design," AIAA Paper No. 2005-4815, June 2005.

[5] Wright, R. L. and Zoby, E. V., "Flight Boundary Layer Transition Measurements on a Slender Cone at Mach 20," AIAA Paper No. 77-719, June 1977.

[6] Vojvodich, N. S., "PAET Entry Heating and Heat Protection Experiment," *Journal of Spacecraft*, Vol. 10, No. 3, March 1973.

[7] Rumsey, C. B., Carter, H. S., Hastings, E. C., Jr., Raper, J. L., and Zoby, E. V., "Initial Results from Flight Measurements of Turbulent Heat Transfer and Boundary Layer Transition at Local Mach Numbers Near 15 (Re-entry F)," TM X-1856, 1966, NASA.

[8] Yamamoto, Y. and Minako, Y., "CFD and FEM Coupling Analysis of OREX Aerothermodynamic Flight Data," AIAA Paper No. 95-2087, June 1995.

[9] Gupta, R. N., Moss, J. N., and Price, J. M., "Assessment of Thermochemical Nonequilibrium and Slip Effects for Orbital Re-entry Experiment (OREX)," AIAA Paper No. 96-1859, June 1996.

[10] Jahn, G., Schöttle, U., and Messerschmid, E., "Post-Flight Surface Heat Flux and Temperature Analysis of the MIRKA Re-entry Capsule," *Proceedings of the 21st International Symposium on Space Technology*, Omiya, Japan, May 1998, pp. 532-537.

[11] Cazaux, C., Watillon, P., and Durand, G., "Atmospheric Re-entry Demonstrator (ARD): A Flight Experiment for Technology Qualification within the European Manned Space Transportation Programme (MSTP)," *Proceedings of the Second European Symposium on Aerothermodynamics for Space Vehicles*, Noordwijk, Netherlands, November 1994, pp. 463-466.

[12] Olds, A. D., Beck, R. E., Bose, D. M., White, J. P., Edquist, K. T., Hollis, B. R., Lindell, M. C., Cheatwood, F. M., Gsell, V. T., and Bowden, E. L., "IRVE-3 Post-Flight Reconstruction," AIAA Paper No. 2013-1390, March 2013.

[13] General Electric, "Measurement & Control – UNIK 5000 Pressure Sensing Platform," 920-4831 Datasheet, 2012.

[14] MEDTHERM Corp., "64 Series Heat Flux Transducers and Infrared Radiometers for the Direct Measurement of Heat Transfer Rates," Bulletin 118, August 2003.

[15] Lee, D. B., Bertin, J. J., Goodrich, W. D., "Heat-Transfer Rate and Pressure Measurements Obtained During Apollo Orbital Entries," TN D-6028, October 1970, NASA.

[16] Grimaud, J. E., Tillian, D. J., "Heat Transfer Rate Measurement Techniques in Arc-Heated Facilities," *ASME 88th Winter Annual Meeting and 2nd Energy Systems Exposition*, Pittsburgh, PA, November 1967.

[17] Yanswitz, H. and Beckman, P., "A Heat-Flux Gage for Use on Recessive Surfaces," ISA Transactions, Vol. 6, No. 3, July 1967, pp. 188-193.

[18] Wright, M. J., Prabhu, D. K., and Martinez, E. R., "Analysis of Afterbody Heating Rates on the Apollo Command Modules, Part 1: AS-202," AIAA Paper No. 2004-2456, June 2004.

[19] Lee, D. B. and Goodrich, W. D., "The Aerothermodynamic Environment of the Apollo Command Module During Superorbital Entry," TN D-6792, April 1972, NASA.

[20] Edquist, K. T., Wright, M. J., and Allen, G. A. Jr., "Viking Afterbody Heating Computations and Comparisons to Flight Data," AIAA Paper No. 2006-386, January 2006.

[21] Edquist, K. T., "Computations of Viking Lander Capsule Hypersonic Aerodynamics with Comparisons to Ground and Flight Data," AIAA Paper No. 2006-6137, August 2006.

[22] Milos, F. S. and Chen, Y. -K. "Mars Pathfinder Entry Temperature Data, Aerothermal Heating, and Heatshield Material Response," AIAA Paper No. 98-2681, 1998.

[23] Spencer, D. A., Blanchard, R. C., Braun, R. D., Kallemeyn, P. H., and Thurman, S. W., "Mars Pathfinder Entry, Descent, and Landing Reconstruction," *Journal of Spacecraft and Rockets*, Vol. 36, No. 3, May – June 1999, pp. 357-366.

[24] Bose, D., White, T., Mahzari, M., and Edquist, K., "Reconstruction of Aerothermal Environment and Heat Shield Response of Mars Science Laboratory," *Journal of Spacecraft and Rockets*, Vol. 51, No. 4, July – August 2014, pp. 1174-1184.

[25] Dutta, S. and Braun, R. D., "Statistical Entry, Descent, and Landing Performance Reconstruction of the Mars Science Laboratory," *Journal of Spacecraft and Rockets*, Vol. 51, No. 4, July – August 2014, pp. 1048-1061.
[26] Bose, D., White, T., Santos, J. A., Feldman, J., Mahzari, M., Olson, M., and Laub, B., "Initial Assessment of Mars Science Laboratory Heatshield Instrumentation and Flight Data," AIAA Paper No. 2013-0908, January 2013.
[27] Bose, D., Santos, J. A., Rodriquez, E., White, T., Olson, M., and Mahzari, M., "Mars Science Laboratory Heat Shield Instrumentation and Arc Jet Characterization," AIAA Paper No. 2013-2778, June 2013.
[28] Milos, F. S., Chen, Y. -K., Squire, T. H., and Brewer, R. A., "Analysis of Galileo Probe Heatshield Ablation and Temperature Data," *Journal of Spacecraft and Rockets*, Vol. 36, No. 3, May – June 1999, pp. 298-306.
[29] "Galileo Probe Mission Operations Final Report," Hughes Space and Communications Co., Rept. HS373-6000, September 1996.
[30] Milos, F. S., "Galileo Probe Heat Shield Ablation Experiment," AIAA Paper No. 96-1823, June 1996.
[31] Mahzari, M., "Inverse Estimation Methodology for the Analysis of Aeroheating and Thermal Protection System Data," PhD Dissertation, Georgia Institute of Technology, December 2013.
[32] Wells, G., "A Comparison of Multiple Techniques for the Reconstruction of Entry, Descent, and Landing Trajectories and Atmospheres," PhD Dissertation, Georgia Institute of Technology, May 2011.

XI. Biography

***Bryce A. Woollard*[1]**

Bryce A. Woollard is currently a graduate student at the Georgia Institute of Technology pursuing his Master's Degree in Aerospace Engineering. He works under the guidance of Dr. Robert D. Braun within Georgia Tech's Space Systems Design Laboratory (SSDL). The primary focus of his research includes thermal protection system instrumentation, as well as small probe design and manufacturing. His scheduled date of graduation is early August 2016, and he plans to transition into industry following graduation.

Robert D. Braun[2]

PLACEHOLDER FOR RDB

Deepak Bose[3]

Deepak Bose is an Aerospace Engineer in the Entry Systems and Technology Division at NASA Ames Research Center. Deepak serves as the Principal Investigator of the Mars Entry Descent and Landing Instrumentation-2 (MEDLI-2) flight instrumentation project for Mars-2020 mission. He also leads post-flight assessment of Orion MPCV Exploration Flight Test-1 thermal protection system. He is a recipient of 2015 and 2011 NASA Outstanding Leadership and 2009 NASA Exceptional Achievement Medals. He has co-authored more than 100 research papers, and has three patents. Deepak received his Ph.D. from University of Minnesota in Aerospace Engineering.